Journal of Nano- and Electronic Physics
Vol. **12** No 1, 01005(6pp) (2020)

Журнал нано- та електронної фізики
Том **12** № 1, 01005(6cc) (2020)

Formation and Physical Properties of Multicomponent Coatings Sputter-deposited from Co-Cr-Ni-Ti-Zr-Hf-Ta-W-C Segmented Target

V.I. Perekrestov[1], Yu.O. Kosminska[1,*], G.S. Kornyushchenko[1], Yu.V. Gannych[1], O. Gedeon[2]

[1] *Sumy State University, 2, Rymsky-Korsakov St., 40007 Sumy, Ukraine*
[2] *Institute of Chemical Technology, 5, Technicka St., CZ-16628 Prague 6, Czech Republic*

(Received 11 November 2019; revised manuscript received 15 February 2020; published online 25 February 2020)

Multicomponent coatings were fabricated by sputtering of a rod target consisting of discs of various metals and carbon. The sputtering device used in this study has been developed by authors and represents modified dc magnetron sputtering with cathodic assembly in the form of a hollow cathode. A pipe is located coaxially to the sputtered rod target, and deposition takes place onto the inner surface of the pipe. In order to study structural and phase state and physical properties of the deposits, substrates are used which are placed along the pipe's inner surface parallel to the rod target axis. For a set of elements of Co, Cr, Ni, Ti, Zr, Hf, Ta, W and carbon to build the segmented rod target, elemental composition of the corresponding coatings on the substrates was studied by means of EDXA. Elemental distribution revealed the formation of $(TiTaW)C_{0.34}$, $(TaTiWCrHf)C_{0.22}$, $(WTaTiCrHfCo)C_{0.12}$, $(CrWHfTaCoNiTiZr)C_{0.1}$, $(CrHfWNiCoTaTi)C_{0.09}$ and $(CrHfNiCoWTa)C_{0.08}$ coatings. From TEM, SEM and XRD studies it was concluded that the coatings structure varied from fine-dispersed polycrystalline to amorphous as carbon concentration increased. Along with it, as carbon concentration reached ~ 22 at. %, the surface roughness increased, solid solution of Ti, Ta, Hf, Cr, W carbidized, and microhardness increased up to 17 GPa. Finally, elemental composition of the coatings can be controlled by varying composition and geometry of the segmented rod target.

Keywords: Multicomponent coatings, Metal carbide coatings, Structure formation, Deposition by sputtering, Segmented target.

DOI: 10.21272/jnep.12(1).01005 PACS numbers: 68.55. – a, 81.15.Cd

1. INTRODUCTION

Evolution of advanced coatings technology is ever more directed at increasing the number of constituent chemical elements. It allows fabricating coatings with unique combination of their functional properties, such as high heat resistance, wear resistance, corrosion resistance, etc.

If to consider deposition of multicomponent coatings with high configurational entropy, they grow in the form of solid solutions in crystalline monophase or amorphous state, as a rule. Physical characteristics and high functional possibilities of high-entropy coatings are determined by the effects of mixing, lowering of atomic interdiffusion, and lattice distortion. To obtain high-entropy state, equiatomic elemental composition is used most often [1]. At the same time, functionality of the coatings can be enhanced using non-equiatomic composition as well [2]. Among the most studied elemental compositions forming multicomponent alloys there are CoCrFeMnNi [3], AlCoCrCuFeNi [4], and $AlCoCrFeNiTi_x$ [5]. Further development of multicomponent coatings technology is related to fabrication of their nitrides [6]. It should be emphasized that multimetal nitrides growth is typically accompanied by fcc phase formation [7]. Thus, in this case one can speak of nitride formation on the basis of solid solution of a multicomponent system while formation of single metal nitrides is impossible.

It can be suggested that further development of multicomponent coatings technology will be closely related to carbidization processes. Since carbon cannot exist in gas form under normal conditions as opposite to nitrogen, creation of carbides of multicomponent systems is more complicated. The number of publications on the nitride coatings significantly prevails over publications related to obtaining the carbides [2, 8]. Along with it, in [9] it is shown that the hardness of multicomponent carbides of transition metals is much higher than the average hardness of their binary constituents. At the same time, carbide multicomponent coatings have high operational characteristics and, therefore, can be used in various fields of science and engineering [10, 11].

In [12], multicomponent (TiZrNbHfTa)N and (TiZrNbHfTa)C coatings were obtained by magnetron sputtering of pure metals Ti, Zr, Nb, Hf and Ta in reactive ambients $Ar + N_2$ and $Ar + CH_4$ correspondingly. Complex study of their mechanical properties showed that (TiZrNbHfTa)C were much better than the nitrides. It should be also mentioned that even little additions of carbon up to 0.5-2.5 at. % to FeCoCrNi high-entropy alloys resulted in the formation of $M_{23}C_6$ carbides and strengthened the material [13, 14].

To deposit multicomponent carbide coatings, magnetron sputtering in chemically active or inert ambient is widely used. In [15], (AlCrTiNbY)C coatings were deposited in $CH_4 + Ar$ ambient. The coatings consisted of intermetallic, carbide, and carbon phases, and had maximum hardness of 23 GPa. In [16], $(CrNbSiTiZr)C_x$ coatings with microhardness of 32 GPa at 36.7 at. % of carbon were fabricated. Carbide coatings of (CrNbTaTiW)C system with microhardness of 36 GPa were deposited by magnetron sputtering of targets of C, Nb, Ti/Cr (1:1) and segmented target Ta/W (1:1) [17].

Hence, one can state the importance of investigation of structure formation mechanisms of multicomponent carbide coatings. At the same time, there is a topical

* y.kosminska@phe.sumdu.edu.ua

technological problem to deposit the coatings on inner surface of low diameter pipes. Therefore, the aim of the present article is to develop a deposition technique for obtaining the coatings on the basis of Cr, Co, Ni, W, Ta, Hf, Zr, Ti and C by means of ion-plasma sputtering of a rod target which is composed of discs of the above chemical elements and located inside a 40 mm diameter pipe.

2. EXPERIMENTAL PROCEDURE

Multicomponent coatings were obtained by sputtering of a rod-like target composed of various metals (Cr, Co, Ni, W, Ta, Hf, Zr, Ti) and carbon. The rod was placed inside a pipe coaxially. In Fig. 1, the mutual arrangement of the discs of different chemical elements within the rod and the external pipe is shown. The discs were of 11 mm in diameter and the distance between centers of the substrates 1 and 6 was 93 mm.

The rod was sputtered by argon ion bombardment formed in the glow discharge. Because of the hollow cathode and magnetron effects, the discharge current was increased and stabilized under relatively low working gas pressure (P_{Ar} = 5 Pa). Detailed structure and basic physics of operation of the rod sputterer were described in [18].

An important feature of the rod sputterer is that the rod target is not cooled [18]. That is why the rod temperature can rise to 650-750 °C even at the discharge power of ~ 450 W, as pyrometric investigations have shown. The increased rod temperature results in the increase of the sputtering coefficient of the rod constituents, and, hence, in the increase of the growth rate of the coatings. Because of the quite short distance between the substrates and the rod surface (~ 15 mm), there is considerable radiation heating of the coatings surface.

Thermocouple measurements showed that the growth surface temperature was within 280-350 °C at the discharge power of 450 W and with the heater 8 off.

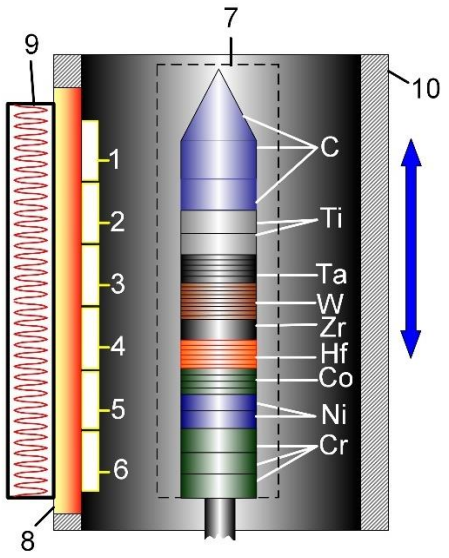

Fig. 1 – Schematic representation of the sputtering device elements (1-6 are the substrates; 7 is the sputtered rod consisting of various metals and carbon; 8 is the substrate holder; 9 is the substrate heater; 10 is the external pipe

Considering the stated above, the technique for depositing the coatings onto the substrates 1-6 was as follows. Initially, the substrate 1 was placed at the level of the chromium discs (see Fig. 1). Then the substrates were heated to 320 °C by the heater 8. Further the sputterer power unit was turned on and the discharge power was fixed at 450 W. At the next stage the deposition of mostly Cr took place onto the substrate 1 during 2 min while the substrates and the rod target were kept mutually immobile. After that the substrates moved gradually along the rod during 12 min to the location as shown in Fig. 1 with simultaneous lowering the power of the heater 8 to zero. Deposition continued onto all the substrates for 2 hours. Thus, the above stages of the experiment allowed depositing Cr at first which was responsible for high adhesion. Further prolonged deposition onto all the substrates at mutually immovable rod and the substrates allowed determining the distribution of elemental and phase compositions of the coatings deposited opposite different rod parts. In future it will give a possibility to predict the thickness distribution of the elemental composition and physical properties of the composite coatings fabricated on inner surfaces of a pipe while the pipe is continuously sliding along the rod. Under such conditions the layers will be formed sequentially with maximal content of Cr, Ni, Co, Hf, Zr, W, Ta, Ti and C. It should be noted that in case of cosine angular distribution of sputtered atoms and their diffusive motion the coatings will possess gradual transitions from one chemical element to another [18]. This fact is a necessary prerequisite for delocalization of inner mechanical stress in the coatings. Besides, gradual turning the heater 8 off eliminates the growth surface heating by thermal radiation of the rod.

Deposition experiments were carried out in purified argon ambient. The coatings of 3.8 μm thick were deposited onto the glass substrates. To perform TEM characterization, thin films of 60-80 nm thick were obtained on freshly cleaved KCl facets. In the latter case we used lower discharge power (~ 330 W) to decrease the growth surface temperature to 230-260 °C. The mutual location of the substrates and the rod corresponded to that in Fig. 1.

Structure and elemental composition of the coatings were studied by scanning electron microscopes FEI NanoSEM 230 and Inspect S50-B using EDX analysis with relative error of 5 %. XRD studies were carried out by ДРОН 4. Electron diffraction and structural studies were performed by transmission electron microscope ПЕМ-125. The Vickers microhardness of the coatings was measured by МПТ-3 with inaccuracy of 4.3-5 % and normal indentation load of 0.196 H.

3. RESULTS AND DISCUSSION

3.1 Elemental Composition of the Coatings

The dependences of the elemental composition of the coatings either on the substrate number (as in Fig. 1) or on the substrate location relatively to the rod are shown in Fig. 2. Numerical values of the elements concentrations are given in Table 1.

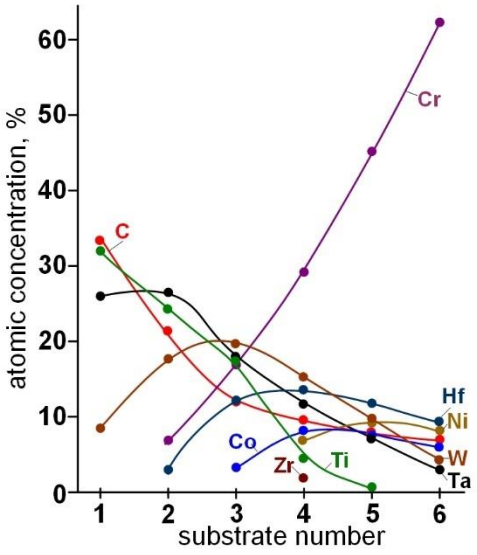

Fig. 2 – Chemical elements concentrations in the coatings versus the substrate numbers

From the given dependences the following can be concluded:

i) Carbon content is found to be nonzero at all the substrates despite its low sputtering coefficient (~ 0.12) that is because of relatively high amount of graphite in the rod (Fig. 1), low carbon atom mass, their possible diffusive movement over long distances, and more intense sputtering of the rod upper part as well.

ii) Nickel and cobalt contents are quite low in the coatings despite their higher sputtering coefficients (~ 1.4 for Ni and 0.4 for Co) and amount in the rod (Fig. 2). After studying the erosion zone of Ni and Co discs, porous structure formation has been found on the surface of these materials which weakens sputtering. It is possibly due to magnetic properties of Ni and Co.

iii) Zirconium has been found only at the substrate 4 that is the most probably related to its low amount in the rod and relatively low sputtering coefficient (~ 0.35).

On the contrary, chromium is present in large amount in the coatings that points out its intense sputtering with the coefficient of ~ 1.3 considering also its increased amount in the rod.

It should also be mentioned that low amount of argon (0.8-2.5 at. %) has been found in all the samples that resulted from Ar implantation to the subsurface layers.

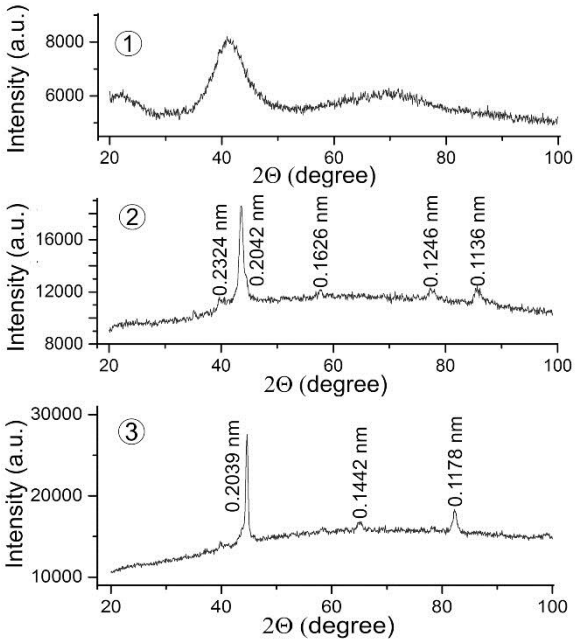

Fig. 3 – Typical XRD patterns of the obtained coatings: 1 – $(TiTaW)C_{0.34}$ (substrate 1), $(TaTiWCrHf)C_{0.22}$ (substrate 2), $(WTa\ TiCrHfCo)C_{0.12}$ (substrate 3), $(CrWHfTaCoNiTiZr)C_{0.1}$ (substrate 4); 2 – $(CrHfWNiCoTaTi)C_{0.09}$ (substrate 5); and 3 – $(CrHf\ NiCoWTa)C_{0.08}$ (substrate 6)

3.2 Structure, Surface Morphology and Phase Composition of the Coatings

Coatings deposited onto glass substrates have been studied by XRD analysis and the results are shown in Fig. 3. Considering mutual location of the substrates and discs of different chemical elements in the rod, and calculated interplanar spacings *d*, one can conclude that the $(CrHfNiCoWTa)C_{0.08}$ coating (substrate 6) includes substantial amount of Cr with corresponding bcc lattice. The most distinctive diffraction peaks in Fig. 3 (substrate 6) are related to (110), (200), and (211) planes of Cr bcc lattice.

Table 1 – Elemental composition of the coatings obtained on different substrates

Chemical element	Substrate No 1, at. %	Substrate No 2, at. %	Substrate No 3, at. %	Substrate No 4, at. %	Substrate No 5, at. %	Substrate No 6, at. %
C	34.02	21.95	12.01	9.14	7.55	7.26
Ti	31.98	25.05	17.02	4.03	0.85	
Cr		6.10	16.30	30.33	46.06	59.22
Co			4.23	8.47	6.95	6.40
Ni				6.25	9.65	8.38
Zr				2.03		
Hf		1.90	11.41	13.51	12.20	10.34
Ta	26.04	27.10	18.39	10.75	6.06	3.16
W	7.96	17.74	19.03	14.38	10.49	4.10
Ar		0.16	1.61	1.11	0.19	1.14

Cr concentration decreases and Co, Ni and Hf concentration increases at transition to the substrate 5. Along with it, the $(CrHfWNiCoTaTi)C_{0.09}$ coating is formed. It has been almost impossible to determine the crystal lattice type because of specific mutual position of the diffraction peaks on the XRD patterns and corre-

sponding interplanar spacings (Fig. 3, substrate 5). Most probably, intermetallic inclusions are formed. Thus, in Fig. 3 (substrate 5) the highest diffraction peak with $d = 0.2042$ nm corresponds most probably to intermetallic compound CrNi whose (211) interplanar spacing has the value of 0.2044 nm. The diffraction peaks that correspond to interplanar spacings 0.2324 nm and 0.1626 nm can belong to CrC ($d = 0.2330$ nm for (111) planes) and Cr_2Hf ($d = 0.1627$ nm for (211) planes) respectively. At the same time, identification of the diffraction peaks with 0.1246 nm and 0.1136 nm has failed.

Considering the substrates 4, 3, 2, and 1 one after another, the transition to an amorphous phase takes place, which can be seen in Fig. 3-1. Amorphization becomes more intense with increase in the carbon content, thus, $(TiTaW)C_{0.34}$, $(TaTiWCrHf)C_{0.22}$, $(WTaTiCrHfCo)C_{0.12}$ and $(CrWHfTaCoNiTiZr)C_{0.1}$ coatings are formed on the substrates 1, 2, 3, and 4 respectively. The mentioned amorphization is determined by solid solution formation provided that different atoms cannot create intermetallic compounds or crystalline inclusions of single metals because of weak interdiffusion. Homogeneously mixed state of different atoms also precludes formation of single metal carbides.

TEM microstructures and electron diffraction patterns are shown in Fig. 4. Comparing XRD and TEM studies, one can conclude that they agree with each other. The electron diffraction patterns of the coating on the substrate 6 have diffraction peaks of Cr bcc lattice that coincides with XRD results (see Fig. 3 and Fig. 4). As both XRD and TEM studies have shown, transition to the structures on the substrate 5 is accompanied by the formation of multiphase crystalline state. Further transition to the coatings on the substrates 4, 3, 2, 1 reveals amorphous phase formation.

From the TEM images related to the substrates 5 and 6 (see Fig. 4) it follows that the coatings have fine-dispersed polycrystalline structure. Besides, there are more and less lightened areas in the main matrix of the deposits which can be attributed to accumulation of different phases. Consecutive increase in the Hf, W, Ta, Ti and C percentage corresponds to the formation of more structurally homogeneous amorphous deposits (see Fig. 2 and Fig. 4, substrates 4, 3, 2, 1).

SEM-studies of the coatings surface morphology are shown in Fig. 5. The SEM images are numerated similar to the substrate numbers. At maximal chromium content on the substrate 6 a developed surface grows in the form of elongated structural elements. Along with it, decrease in Cr content in the coatings on the substrate 5 changes the surface morphology considerably. In this case rounded clusters instead of the elongated structures are observed.

Surface morphology of the coatings that include all the chemical elements on the rod and is obtained on the substrate 4 (Fig. 2) features a system of convex clusters on a relative smooth surface. Most probably the clusters are formed because of the field selectivity which is characteristic for amorphous deposits [19].

Further change of the elemental composition through decrease in Cr content and increase in Hf, W, Ta, Ti, C content gradually creates the prerequisites for smooth surface formation (Fig. 5, substrates 3, 2, 1).

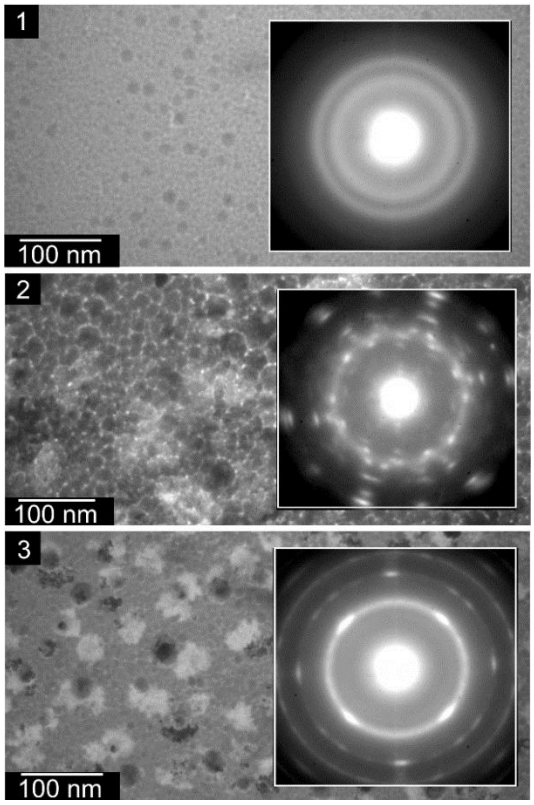

Fig. 4 – Microstructure and electron diffraction patterns obtained by TEM studies of the multicomponent coatings: 1 – $(TiTaW)C_{0.34}$ (substrate 1); 2 – $(CrHfWNiCoTaTi)C_{0.09}$ (substrate 5); 3 – $(CrHfNiCoWTa)C_{0.08}$ (substrate 6); structure and diffraction patterns for coatings on substrates 2, 3 and 4 are close to those for the substrate 1

Such surface transformation agrees with the corresponding transition to more homogeneous structures revealed by TEM studies (Fig. 4-1).

In the coatings on the substrate 2 there are dark inclusions that draw attention. To investigate their nature, additional SEM studies were performed in the reflected electron mode. Since under this mode the contrast from the dark inclusions has disappeared (see Fig. 5, substrate 2, small image "a"), one can suggest homogeneity of the elemental composition of the inclusions and the matrix. From this it follows that the dark inclusions in the SEM images obtained under secondary electron mode result from specific structural features.

3.3 Microhardness of the Coatings

Microhardness measured in the middle of the substrates depends considerably on the elemental composition or the substrate number (Fig. 6).

The major impact in the microhardness increase up to 17 GPa for the $(TaTiWCrHf)_1C_{0.22}$ coatings belongs to the increase in carbon content. Obviously, such increase in the microhardness is caused by the formation of a carbide of HfWTaTi mixture. The fact of relatively low microhardness of $(TiTaW)_1C_{0.34}$ coatings obtained on the substrate 1 at the highest carbon content draws one's attention. Such a discrepancy can be explained by weak plasma flux onto the substrate 1 and thus ineffective carbidization.

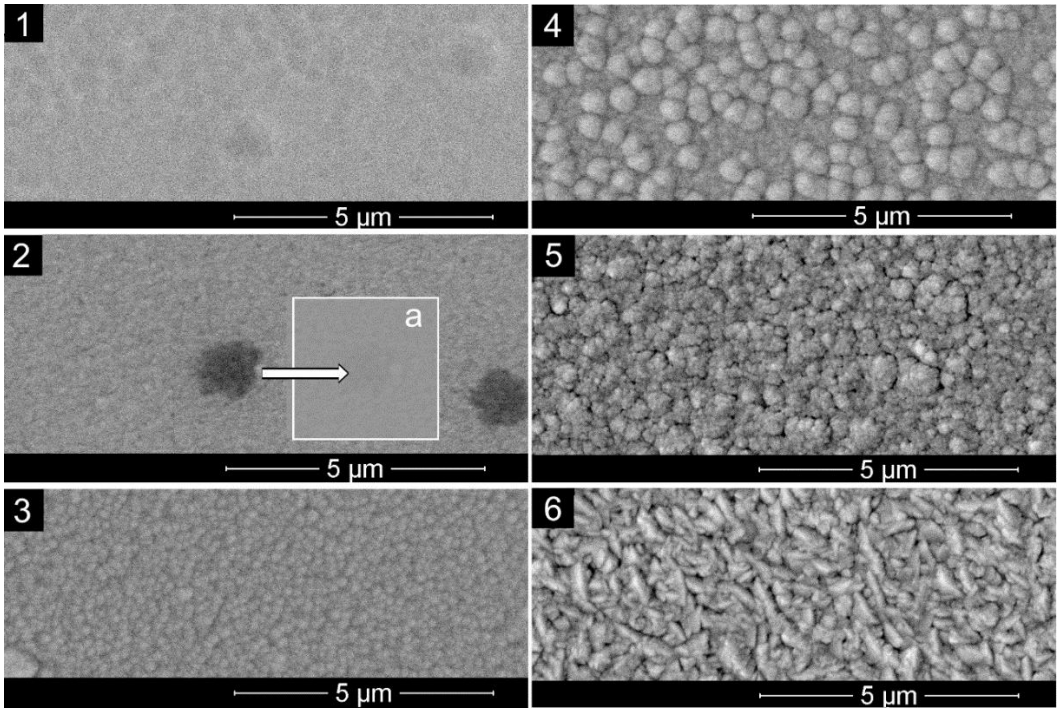

Fig. 5 – SEM images of the surface morphology of the multicomponent coatings $(TiTaW)C_{0.34}$ (substrate 1), $(TaTiWCrHf)C_{0.22}$ (substrate 2), $(WTaTiCrHfCo)C_{0.12}$ (substrate 3), $(CrWHfTaCoNiTiZr)C_{0.1}$ (substrate 4), $(CrHfWNiCoTaTi)C_{0.09}$ (substrate 5), and $(CrHfNiCoWTa)C_{0.08}$ (substrate 6), the coatings were ~ 3.8 μm thick. Image "a" for the substrate 2 was obtained under the reflected electron mode

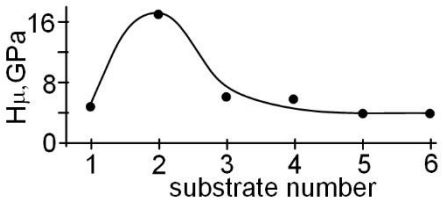

Fig. 6 – Microhardness of the coatings measured in the middle of the substrates versus the substrate number: $(TiTaW)C_{0.34}$ (substrate 1); $(TaTiWCrHf)C_{0.22}$ (substrate 2); $(WTaTiCrHfCo)C_{0.12}$ (substrate 3); $(CrWHfTaCoNiTiZr)C_{0.1}$ (substrate 4); $(CrHfWNiCoTaTi)C_{0.09}$ (substrate 5); $(CrHfNiCoWTa)C_{0.08}$ (substrate 6)

4. CONCLUSIONS

1. The following multicomponent coatings were deposited by ion-plasma sputtering of a segmented rod consisted of Cr, Ni, Co, Zr, Hf, W, Ta, Ti and C discs: $(TiTaW)C_{0.34}$, $(TaTiWCrHf)C_{0.22}$, $(WTaTiCrHfCo)C_{0.12}$, $(CrWHfTaCoNiTiZr)C_{0.1}$, $(CrHfWNiCoTaTi)C_{0.09}$, $(CrHfNiCoWTa)C_{0.08}$ on the substrates 1-6 respectively.

2. SEM, TEM and XRD studies revealed fine-dispersed polycrystalline structure of $(CrHfNiCoWTa)C_{0.08}$ and $(CrHfWNiCoTaTi)C_{0.09}$ coatings with the grain size of a few nanometers. The $(CrHfNiCoWTa)C_{0.08}$ coatings included bcc Cr lattice, and the crystalline structure of the $(CrHfWNiCoTaTi)C_{0.09}$ coatings was most probably due to the formation of intermetallic compounds.

3. The coatings with high carbon content such as $(TiTaW)C_{0.34}$, $(TaTiWCrHf)C_{0.22}$, $(WTaTiCrHfCo)C_{0.12}$ and $(CrWHfTaCoNiTiZr)C_{0.1}$ were obtained in the form of structurally and morphologically homogeneous amorphous phase with increased microhardness (~ 17 GPa for $(TaTiWCrHf)C_{0.22}$).

ACKNOWLEDGEMENTS

The present work was funded by Ukrainian State Budget within the project No. 0118U003573.

REFERENCES

1. Sh. Guo, C.T. Liu, *Prog. Nat. Sci–Mater.* **21**, 433 (2011).
2. B.S. Murty, J.W. Yeh, S. Ranganathan, P.P. Bhattacharjee, *High-Entropy Alloys* (Elsevier: 2019).
3. Sh. Yin, W. Li, B. Song, X. Yan, M. Kuang, Y. Xu, K. Wen, R. Lupoi, *J. Mater. Sci. Tech.* **35**, 1003 (2019).
4. T.-T. Shun, Y.-Ch. Du, *J. Alloy Compd.* **479**, 157 (2009).
5. Y. Wang, Sh. Ma, X. Chen, J. Shi, Y. Zhang, J. Qiao, *Acta Metall. Sin.–Eng.* **26**, 277 (2013).
6. C.H. Lai, M.H. Tsai, S.J. Lin, J.W. Yeh, *Surf. Coat. Technol.* **201**, 6993 (2007).
7. A.D. Pogrebnjak, A.A. Bagdasaryan, I.V. Yakushchenko, V.M. Beresnev, *Russ. Chem. Rev.* **83,** 1027 (2014).
8. D.B. Miracle, O.N. Senkov, *Acta Mater.* 122, 448 (2017).
9. T.J. Harrington, J. Gild, P. Sarker, C. Toher, Ch.M. Rost, O.F. Dippo, C. McElfresh, K. Kaufmann, E. Marin, L. Borowski, P.E. Hopkins, J. Luo, S. Curtarolo, D.W. Brenner, K.S. Vecchio, *Acta Mater.* **166**, 271 (2019).
10. J.-W. Yeh, S.-J. Lin, *J. Mater. Res.* **33**, 3129 (2018).
11. E. Abbasi, K. Dehghani, *J. Alloy Compd.* **783**, 292 (2018).
12. V. Braic, A. Vladescu, M. Balaceanu, C.R. Luculescu, M. Braic, *Surf. Coat. Technol.* **211**, 117 (2012).

13. L. Guo, X. Ou, S. Ni, Y. Liu, M. Song, *Mater. Sci. Eng. A.* **746**, 356 (2019).
14. J.Y. Ko, S.I. Hong, *J. Alloys Compd.* **743**, 115 (2018).
15. M. Braic, V. Braic, M. Balaceanu, C.N. Zoita, A. Vladescu, E. Grigore, *Surf. Coat. Technol.* **204**, 2010 (2010).
16. Y.-S. Jhong, Ch.-W. Huang, S.-J. Lin, *Mater. Chem. Phys.* **210**, 348 (2018).
17. P. Malinovskis, S. Fritze, L. Riekehr, L. von Fieandt, J. Cedervall, D. Rehnlund, L. Nyholm, E. Lewin, U. Jansson, *Mater. Design* **149**, 51 (2018).
18. Yu.O. Kosminska, V.I. Perekrestov, G.S. Kornyushchenko, *Metallofiz. Nov. Tech.* **41(6)**, 733 (2019).
19. Yu.O. Kosminska, A.A. Mokrenko, V.I. Perekrestov, *Tech. Phys. Lett.* **37**, 538 (2011).

Формування та фізичні властивості багатокомпонентних покриттів, отриманих шляхом розпилення складеної мішені з Co-Cr-Ni-Ti-Zr-Hf-Ta-W-C

В.І. Перекрестов[1], Ю.О. Космінська[1], Г.С. Корнющенко[1], Ю.В. Ганніч[1], О. Гедеон[2]

[1] *Сумський державний університет, вул. Римського-Корсакова, 2, 40007 Суми, Україна*
[2] *Інститут хімічних технологій, вул. Технічна 5, CZ-16628 Прага 6, Чехія*

Шляхом розпилення мішені-стрижня, що складається з шайб різних металів та вуглецю, отримані багатокомпонентні покриття. Розпилювальний пристрій, що використовувався для отримання покриттів, був розроблений авторами та є модифікацією магнетронного розпилення на постійному струмі з катодним вузлом у вигляді пустотілого катода. Коаксіально розпилювальній мішені-стрижню розташовують трубу, на внутрішню поверхню якої відбувається конденсація. З метою досліджень структурно-фазового стану та фізичних властивостей конденсатів використовують підкладки, які розташовують вздовж внутрішньої поверхні труби паралельно осі мішені-стрижня. На основі вивчення методом EDXA розподілу елементного складу конденсатів на таких підкладках за використання набору шайб з металів Co, Cr, Ni, Ti, Zr, Hf, Ta, W та вуглецю встановлено формування покриттів $(TiTaW)C_{0.34}$, $(TaTiWCrHf)C_{0.22}$, $(WTaTiCrHfCo)C_{0.12}$, $(CrWHfTaCoNiTiZr)C_{0.1}$, $(CrHfWNiCoTaTi)C_{0.09}$ та $(CrHfNiCoWTa)C_{0.08}$. При дослідженні покриттів за допомогою ПЕМ та РЕМ, а також рентгенофазового аналізу зроблено висновок про те, що їх структура при збільшенні вмісту вуглецю змінюється від дрібнодисперсних полікристалів до аморфного стану. З підвищенням концентрації вуглецю приблизно до 22 ат. % відбувається зменшення шорсткості поверхні покриттів, карбідизація твердого розчину Ti, Ta, Hf, Cr, W та відповідне підвищення мікротвердості покриттів до 17 ГПа. Насамкінець, елементним складом покриттів можна керувати, варіюючи склад та геометричні параметри складеної мішені-стрижня.

Ключові слова: Багатокомпонентні покриття, Металокарбідні покриття, Структуроутворення, Осадження розпиленням, Складена мішень.